Improvements in the Prediction of Steady and Unsteady Transition and Mixing in Low Pressure Turbines By Means of Machine-Learnt

IMPROVEMENTS IN THE PREDICTION OF STEADY AND UNSTEADY TRANSITION AND MIXING IN LOW PRESSURE TURBINES BY MEANS OF MACHINE-LEARNT CLOSURES

Roberto Pacciani
Michele Marconcini*
Andrea Arnone
Department of Industrial Engineering
University of Florence, Italy
Email: michele.marconcini@unifi.it

Francesco Bertini
Ennio Spano
Simone Rosa Taddei
GE Avio,
Rivalta di Torino, Italy
francesco.bertini@avioaero.it

Richard D. Sandberg
Department of Mechanical Engineering
University of Melbourne, VIC, 3010, Australia
richard.sandberg@unimelb.edu.au

ABSTRACT

In this paper novel machine-learnt transition and turbulence models are applied to the prediction of boundary-layer transition and wake-mixing in a Low-Pressure Turbine (LPT) cascade, including unsteady inflow cases with incoming wakes. A Laminar Kinetic Energy (LKE) transport approach is employed as baseline transition framework. The application of the machine learnt EARSMs takes advantage of a zonal strategy based on a newly developed sensing function that allows automated wake demarcation. This work compares the performance of several approaches that are based on the application of improved transition models without machine learnt EARSMs, baseline transition model with EARSMs trained for improved wake mixing, and new transition and turbulence closures that are simultaneously developed in a fully coupled way and aimed at improving both transition and wake mixing predictions in LPTs. The investigation is carried out on a cascade of industrial footprint, representative of modern LPT bladings. First of all, the various modelling frameworks are evaluated, without bar wakes (steady conditions), over a wide range of Reynolds number values. URANS analyses have also been carried out to investigate the predictive capabilities of machine-learnt closures in the presence of incoming bar wakes. RANS/URANS results are scrutinized against LES calculations and experimental data. It will be demonstrated that machine learnt EARSMs are capable of producing realistic wake mixing when simply applied on top of the baseline transition models. However, the most accurate predictions will be shown to be provided by fully integrated machine-learnt transition/turbulence closures.

*Address all correspondence to this author.

INTRODUCTION

In order to transform global air transport towards a sustainable and climate neutral future, breakthrough technology initiatives must be pursued for the introduction of new and cleaner aeroengines by 2030. These initiatives aim to reduce greenhouse gas emissions from aircrafts by at least 30%, compared to the 2020 state-of-the-art technology, in an effort to pave the way towards climate-neutral aviation by 2050 (source: `http://www.clean-aviation.eu`, accessed on November 2022). However, CO_2 emissions are not alone in challenging the expansion of air traffic, as aircraft noise is one major concern for the construction of new airports, or the expansion of existing ones. A technology initiative that has a direct impact the carbon footprint of aeroengines is fuel saving. Noise reduction at the source has proven to be effective and thus it remains one of the primary objectives for the aviation industry. Clearly, there is no such thing like an obvious but brilliant solution for the speed-up of aircraft engines technology towards an emissions-free design, but a number of different avenues must be explored. Among these, the improvement of engine components design remains a promising one.

The low pressure turbine (LPT) is one of the most important component of aircraft engines, as it drives their overall efficiency. Michelassi et al. [1] reported that, if the LPT efficiency increases by 1% the specific fuel consumption decreases by 0.6%-0.8%, and this implies relevant fuel saving and reduction in emissions. The Reynolds numbers that characterize the operation of traditional LPTs for aeroengines decrease from some hundred thousands at take-off, to less than 10^5 at cruise conditions. In such conditions, a laminar flow regime affects a major portion of the blade boundary-layer, and transition usually occurs in the diffusing part of the blades' suction side. In highly loaded bladerows, transition is often triggered by laminar separation. In the engine multistage environment, bladerow interference effects, that for LPTs are mainly realized in the form of potential and wake interactions, result in unsteady transition dynamics [2]. The boundary layer transition path plays a crucial role in order to determine the overall loss of efficiency of an LPT [3]. For highly loaded bladings, where relevant separation bubbles occur in the absence of incoming disturbances, profile losses undergo significant changes (even reductions) when upstream wakes are present. It's the relative importance of wake induced transition, transition path between wakes, and calming effect [3] that determines the time-averaged overall loss level. The impact of each of those features depend on the wakes reduced frequency and flow coefficient, through the physics of wake/boundary-layer interactions. Praisner et al. [4] reported that losses due to wake mixing can additionally contribute up to 1.5% of efficiency reduction in LPTs. Wake interactions are also a major source of tonal noise emission. The accurate prediction of both transition and wake mixing is therefore of paramount importance in the design phase.

With the fast-pacing power increase computational resources have faced in the last decades, high-fidelity simulations have become feasible [5]. They are able to provide accurate transition and wake mixing predictions [1]. However, such simulations are still not viable for industrial design iterations, due to the high computational cost [6]. Thus, as of today and probably for the next decade, gas turbine design is going to keep on relying on RANS/URANS methods, as they are cost-effective flow modelling tools for engineering solutions.

In the recent past, several modelling proposals have been made to improve transition prediction in RANS/URANS approaches (see Dick et al. [7] for a comprehensive review). A class of transition closures that has recently gained momentum is the one that uses the laminar kinetic energy (LKE) concept [8, 9] in order to address the growth of pre-transitional fluctuations. However, such models are not general or accurate enough for predicting steady and unsteady transition in LPTs. Besides this, the known lack of turbulent diffusion in wake regions, affecting linear eddy viscosity turbulence models (Marconcini et al. [10]), prevents RANS/URANS approaches to be able to provide realistic representations of the mixing phenomenon. Michelassi and Wissink [11] showed that the wake, when being swallowed into the blade passage, undergoes distortion and reacts to the alignment or misalignment of the strain-rate tensor with the Reynolds stress tensor. This suggests that the Bousinnesq approximation should be overcome for a realistic capturing of the wake/blade interaction details.

A promising avenue for amending the deficiencies of RANS/URANS approaches, while maintaining their cost-benefit, is represented by data-driven machine learning for the development of improved turbulence and transition models. A comprehensive overview of existing data-driven methods for turbulence model development can be found in [12].

In 2016, Weatheritt and Sandberg [13] proposed the use of Gene Expression Programming (GEP) [14] for turbulence modeling. Galilean invariant, non-linear closures known as explicit algebraic Reynolds stress models (EARSM) were developed. EARSMs are a computationally efficient way to correct the deficiencies of the Boussinesq approximation. The GEP algorithm produces tangible symbolic expressions that allow a physical interpretation of the involved terms [15]. These expressions can also be directly inserted into RANS codes [16, 17]. EARSMs generated by GEP algorithms have demonstrated to be effective for enhancing the wake mixing prediction in LPTs [18].

In contrast, only a few studies have been conducted in order to improve accuracy of transition models with machine learning [19–21].

Zhao et al. [22] introduced a novel 'CFD-driven' (computational fluid dynamics) framework for EARSM development and used LPTs and high pressure turbines wake flows as training and test cases. Akolekar et al. [23] recently proposed a multi-expression and multi-objective extension to the 'CFD-driven' framework for developing fully coupled transition and turbulence models in a simultaneous way. The base transition modelling framework is represented by the LKE transport approach proposed by Pacciani et al. [9].

It must be pointed out how the majority of the studies regarding transition and turbulence models development via machine-learning report information on the adopted technique and training results, but very few of them discuss a cross-validation of the models in cases different from the training ones. An example of a thorough assessment of a machine-learnt EARSM closure on a LPT cascade, over a range of Reynolds numbers, is reported in Pacciani et al. [18].

The present study is devoted to detailed validation of two different transition/turbulence modelling frameworks created using GEP-based techniques [21, 23]. The first one consists of the application of the EARSM presented in [21] on top of the baseline $k_\ell - k - \omega$ model by Pacciani et al. [9, 24, 25]. The second one is based on the fully integrated transition and EARSM closures proposed in [23]. The investigation is carried out on a cascade of industrial footprint, designed by GE Avio to be representative of modern LPT bladings. The modelling frameworks are initially evaluated in steady conditions, over a wide range of Reynolds number values (from 70k to 300k, in terms of exit isentropic Reynolds number). Most of the considered conditions are far from the training environment of the proposed closures, and such an extended simulation campaign is intended to assess their generality and robustness. URANS analyses are also performed in order to investigate the predictive capabilities of the considered models in unsteady conditions brought about by incoming wakes generated with upstream bars. The machine-learnt EARSMs, that are used to improve wake mixing predictions, are applied via a fully automated zonal strategy that takes advantage of a wake/boundary layer sensing function like in [23]. This is used to identify wake affected regions, where EARSMs are to be applied, while excluding the blade boundary layers, which are to be treated by the transition/turbulence model. Experimental data coming from an extensive test activity carried out at the University of Genoa, and precursor LES analyses performed by GE Avio, with steady and unsteady inflow conditions, enabled a comprehensive and detailed assessment of the CFD predictions.

Indeed, this study presents several novelty aspects. First of all, recently proposed machine-learnt transition/turbulence models are applied for the flow prediction in a modern LPT cascade of industrial design, rather than against common academic test-cases, and over a wide range of operating conditions. The performance of the models in unsteady wake/blade interaction predictions is also discussed, and this is the first known study to report such an investigation. Finally, all the analyses discussed in the paper have been carried out in a fully automated way thanks to the adoption of the wake/boundary-layer sensing function and this also represents a novel contribution. Besides the relative merits of the models in capturing the effects of the flow physics at work in an LPT cascade operating at engine representative conditions, also the robustness of the computational framework on the whole is investigated. Both these aspects are of paramount importance for the feasibility of machine-learnt closures for engineering flow predictions, especially if a prompt penetration of such methodologies into industrial design systems is sought. It is worthwhile to stress how the discussed computational framework has proven to be robust and reliable and how steady and unsteady calculations can be carried out without any relevant and time-consuming user adjustment in models or sensing function parameters. It will be shown how the fully coupled transition/turbulence closure yields superior accuracy for both steady and unsteady calculations, and this suggests that multi-expression, multi-objective, and probably multi-case GEP-based machine-learning techniques represent the most promising route for further model improvements.

TEST CASE AND BOUNDARY CONDITIONS

The cascade analyzed in the present work is representative of a modern LPT vane for aeroengine applications, in terms of blade loading distribution, pitch/chord ratio, Zweifel coefficient, and suction side diffusion rate [18]. The actual profile geometry is confidential and protected by a NDA with the industrial partner, so, in visualizations showing the blade row, it will be reported not to scale. The cascade was experimentally investigated in the blow-down wind tunnel installed at the Aerodynamics and Turbomachinery Laboratory of the University of Genova under a variety of Reynolds number values and inlet conditions, including unsteady conditions with incoming bar wakes. Details on the experimental set-up can be found in Simoni et al. [26] and Marconcini et al. [27]. The measurement campaign considered for the present study covers a range of exit isentropic Reynolds numbers that goes from 0.7×10^5 to 3.0×10^5. The exit isentropic Mach number was about 0.1, so the flow through the cascade was essentially incompressible. Inlet freestream turbulence was generated by a grid placed upstream the cascade and the FSTI considered for the present analysis has a value of 4.2% at the cascade leading edge. For the turbulent length scale, a non-dimensional value of $\ell_T / L_{ref} = 1.6 \times 10^{-3}$, where the axial chord at hub is assumed as the reference length, has been adopted on the basis of previous experiences on the same test rig and experimental set-up [18].

The moving bars wake generator was located 40% axial chord upstream of the cascade leading edge. It was designed to provide values of reduced frequency ($f_{\text{red}} = U_{bar} L_{ref} / (V_{2,is} S_{bar}) = 0.69$) and flow coefficient ($\phi = v_x / U_{bar} = 0.68$) that are representative of engine conditions. The bar/blade count ratio was 2:3.

COMPUTATIONAL FRAMEWORK

The TRAF code [28] was used for all the calculations presented in the paper. It is an in-house developed, density-based, RANS/URANS solver. Incompressible flows are handled via the artificial compressibility method proposed by Chorin [29]. In terms of numerical fluxes, a formally third-order TVD framework, based on the generalized min-mod limiter [30], built on top of the Roe upwind scheme, was employed. For time-accurate calculations a dual time stepping strategy, like in [31–33] has been adopted.

As already mentioned in the Introduction section of the paper, three different transition/turbulence closures have been considered. They are all based on the $k_\ell - k - \omega$ model proposed by Pacciani et al. [9] which combines a laminar kinetic energy transport approach for transition prediction with the Wilcox $k - \omega$ model [34] to obtain a three-equation transition/turbulence closure. Such a model, which has also been employed in the present work, will be referred to as the Baseline model. The second considered closure employs a machine-learnt EARSM that was generated, by virtue of the already mentioned GEP approach, with the aim of improving wake mixing in LPTs. Detailed discussions concerning the EARSM closure can be found in Akolekar et al. [21], and Pacciani et al. [18]. The third model that will be investigated in this paper consists in a machine-learnt closure for fully coupled transition and wake mixing predictions in

LPTs [23]. It was developed through a simultaneous training of the transition and turbulence models, namely the LKE transport equation and a dedicated EARSM closure, by means of a Multi-Expression Multi-Objective (MEMO) strategy based on the GEP algorithm. For this reason this model will be referred to as MEMO model. For sake of clarity, the fundamental difference between the two considered machine-learnt closures must be pointed out. The GEP model consists on the machine-learnt EARSM closure simply being applied on top of the Baseline one, in the MEMO model the LKE equation is formulated differently from the Baseline one and it is fully integrated with its companion EARSM closure. Figure 1 reports a sketch of the CFD-driven GEP algorithm used for models generation. Initially, the GEP algorithm is used to generate a number of colonies. Each colony contains expressions for the EARSM model coefficient (GEP model), or such expressions plus the functional formulations for the production and transfer terms of the LKE model in the MEMO algorithm [21, 23]. All the colonies are run as candidate solutions in parallel CFD calculations. Pitchwise profiles of total pressure loss downstream of the blade trailing edge are then extracted from converged CFD solutions and used to construct a cost function for model evaluation. In addition to this, in the MEMO algorithm, blade surface distributions of C_p and τ_w are also extracted and evaluated against two additional cost functions aimed at improving the transition model. Then, the entire process goes on iteratively for a number of generations and one of the advantages of this process is that it incorporates real-time CFD-feedback into the model development process. In the MEMO case, this resulted in a family of final solutions, and the best candidate was found from the analysis of Pareto fronts (see [23] for the model details). The models were trained against the T106A cascade at $Re_{2,is} = 1.0 \times 10^5$ with DNS results as ground truth data. The GEP model has been a-posteriori assessed in steady conditions against the same LPT blade section discussed in the present work, which features a substantially different design and load distribution relative to the T106 [18]. Such a validation was carried out over a range of operating conditions, and the model application resulted in a striking improvement in terms of wake-mixing predictions at both lower and much higher Reynolds number values relative to the training one.

In both steady and unsteady calculations, the EARSM components of the machine-learnt models are applied by means of an automated zonal strategy based on a sensing function that identifies the wake-affected regions of the flowfield [23]. In steady calculations, the wake sensing function is used to effectively demarcate the wake downstream of the blade trailing edge, like in [23]. In unsteady calculations with upstream rotating bars, the wake sensing function is used for wake demarcation upstream, inside and downstream the blade passage. This allows the application of machine-learnt EARSMs in any wake affected region of the computational domain in a fully automated way. As said, the EARSMs were generated in steady flow conditions to improve wake mixing through the introduction of machine-learnt anisotropic, non-linear terms in the Reynolds stress tensor, as suggested by Pope [35]. The turbulence anisotropy that develops in the wake segments chopped by the blades, as they elongate and stretch while being convected inside the vane passage, is expected to be different from the one arising in the wake generated by the blades and in the upstream ones. Nonetheless, it was considered interesting to investigate the effects of the machine-learnt EARSM closures in terms of robustness of the computational setup on the whole, and on their impact on the unsteady wake/boundary-layer interaction pattern, mixing, and the related loss level. Akolekar et al. [15] suggested that, for a realistic reproduction of the periodic evolution of wake-induced transition phenomena occurring in low pressure turbine cascades, EARSM models should be separately trained in a number of different phases of the wake/blade interaction. Consequently, each model should then be applied in a selected fraction of the wake passing period. The current study was then expected to highlight the feasibility of training strategies of EARSMs for unsteady flows that are simpler, and more amenable for applications. Promising results from the present approach could imply the possibility of generating models on a region-by-region basis (e.g. different closures for regions upstream, inside, and downstream the blade passage) and not on a phase-by-phase basis. It could also address the feasibility of a single model training by using a multi-objective approach that employs suitable cost functions for flow quantities of interest in each selected region of the computational domain.

Wall-resolved LES results were provided by GE Avio. They were carried out by means of the commercial code STAR-CCM+, for both steady and unsteady inflow cases, focusing on lowest Reynolds number case ($Re_{2,is} = 0.7 \times 10^5$) mostly to reduce the computational effort. The spatial discretization was based on a second order segregated numerical scheme with bounded differencing. For the integration in times a second order implicit scheme was adopted. The WALE scheme [36] was used as subgrid scale model, and inlet turbulence was generated via the Synthetic Eddy Method (SEM) [37]. The 2D-Extruded Polyhedral mesh ensures y+ values of the mesh nodes closest to the wall of approximately 0.2, while x^+ and z^+ values are around 10 and 15 all over the computational domain. Three flow-trough times were covered for initialization and 4 for averaging. In the unsteady inflow setup, the upstream moving bars were included in the computational domain. This allowed the extraction of pitchwise distributions of phase-averaged quantities to be used as time-varying inlet boundary conditions for URANS calculations. Such an approach was adopted in order to guarantee physical consistence and high accuracy of the incoming wake characteristics for URANS calculations. As the bar/blade count ratio is 2:3, the period T for unsteady calculations is defined as the time needed for two bars to span three blade pitches. This corresponds to two wake passings for each blade, the bar passing period T_{bars} being equal to $T/2$. The period was discretized with 800 physical time steps, on the base of previous experiences [38].

DOMAIN DISCRETIZATION

Due to the high aspect ratio of the blade, RANS and URANS studies were carried out on the midspan section of the cascade by means of two-dimensional calculations. The cascade flow domain was discretized using an H-O-H grid with 621 mesh points on the blade surface, and 101 in the pitchwise direction for a total of about 150K cells. The H blocks, stitched to the inlet and outlet boundaries of the O mesh, are characterized by uniform mesh spacing in the axial and tangential directions in order to allow optimal resolution in wake-affected regions, avoiding the smearing of the incoming ones and ensuring a realistic representation of mixing phenomena. For the Reynolds numbers considered in the present work, the y+ value of the grid nodes closest to the blade surface is between 1 and 2. The grid structure was selected on the basis of previous experience and validation for cascade flows in incompressible and subsonic conditions and low or moderate Reynolds number [10, 18, 21, 25], while the mesh size was established on the base of a grid dependence analysis. Three grids were generated by approximately halving and doubling the number of mesh points of the reference one along the blade profile and in the pitchwise direction. The dimensions of the coarse (G1), reference (G2), and fine (G3) grids are reported in Tab. 1. The grid dependence analysis is discussed, for steady calculations with the MEMO model at $Re_{2,is} = 0.7 \times 10^5$, in terms of wall shear-stress distributions (Fig. 2(a)) and wake loss profiles (Fig. 2(b)). The results for the G2 and G3 meshes are practically coincident, and this suggests that grid independence is already reached on the reference grid (G2). Predictions for the G1 grid are not very far from the finer grids ones, but discrepancies are detected in the wake loss peak and in the transition region for the wall shear-stress. For URANS calculations with upstream bar wakes, the computational domain comprises three blade passages in order to cope with the actual bar/blade count ratio.

DISCUSSION OF RESULTS

Steady Results

For all the considered Reynolds numbers, transition occurs on the blade suction side due to laminar boundary layer separation. Such circumstance was confirmed by previous unpublished LES studies. Figure 3 compares experimental and computed results at the lowest value of the Reynolds number ($Re_{2,is} = 0.7 \times 10^5$) in terms of blade surface pressure coefficient. Calculated C_p distributions show a general good agreement with measurements, with a clear evidence of boundary layer-separation starting from about $s/s_{tot} = 0.7$, and pressure recovery after transition onset starting from approximately $s/s_{tot} = 0.9$ on the blade suction side. Actually, in the last 10% of the suction surface length, discrepancies arise among the numerical results, with the Baseline model predicting a sharper reattachment relative to both the MEMO model and LES. Remarkably, LES and MEMO simulations predict the same C_p value at the blade trailing edge, which is slightly higher than the one reported by the Baseline calculation. The lack of experimental data on the trailing edge does not allow to assess the ability of the numerical results to reproduce the correct base pressure level, however, it can be argued that both LES and MEMO, unlike the Baseline model, predict a long bubble and, consequently, a lower base pressure. Actually, LES results show a reattachment point which is located just at the trailing edge, as witnessed by the suction side wall shear-stress distributions reported in Fig. 4. It can also be appreciated how the Baseline prediction exhibits an earlier transition relative to the other numerical approaches, with a much pronounced peak at the transition onset location. Flow reattachment also occurs earlier in the Baseline than in the other simulations. In fact, the Baseline model shows the largest TKE production in the trailing edge region. The agreement between LES and MEMO wall shear-stress distributions is remarkable. Although the separation point in the MEMO results is located slightly upstream the one detected by LES, the transition onset locations, identified by the τ_w peaks, are practically coincident for the two simulations. The peak values are also identical and the τ_w behaviour after transition is only marginally different in LES and MEMO predictions, with the latter one showing a slightly delayed reattachment. The capability of the MEMO model to give a realistic evolution of the wall shear-stress in transitional separated flow regions was one of the objectives of its training, as reported in Akolekar at al. [23], and it finds confirmation in the present work. Such a good performance is even more encouraging given that the MEMO model was developed on T106 training data at a different Reynolds number ($Re_{2,is} = 1.0 \times 10^5$).

Further insights on the suction side boundary-layer features reproduction by the RANS approaches can be gained from Fig. 5, where suction side distributions of shape factor (Fig. 5a), and momentum thickness (Fig. 5b) are compared. Both the Baseline and MEMO predictions are in good agreement with the LES results (at least in the fraction of the suction side length where these ones are available). The higher peak in the shape factor (H_{12}) distribution occurring at approximately $s/s_{tot} = 0.9$ (i.e. the transition onset location) possibly indicates the detection of a marginally thicker bubble by the RANS approaches as compared to LES. The slightly higher momentum thickness predicted by the Baseline model at the blade trailing edge with respect to the MEMO model is consistent with the higher turbulence level given by the former one in the last 5% of the suction side length.

In terms of predicted blade loading distributions the agreement with experimental data was found to be satisfactory over the entire range of analyzed Reynolds numbers. For example, Fig. 6 reports blade surface C_p distributions for $Re_{2,is} = 1.5 \times 10^5$ (Fig. 6a) and $Re_{2,is} = 3.0 \times 10^5$ (Fig. 6b). As expected, the separation bubble size decreases when increasing the Reynolds number. There are small differences between the results by the two RANS models and they mainly concern the C_p behaviour in the separation bubble, with the MEMO model consistently predicting a smoother pressure recovery relative to the Baseline one. As expected, GEP predictions were found to lie just on top of the Baseline ones and were not reported in Figs. 3, 4, 5, and 6.

Figure 7 reports calculated and measured pitchwise profiles of total pressure loss coefficient in a section taken $33\%C_x$ downstream of the blade trailing edge for $Re_{2,is} = 0.7 \times 10^5$ (Fig. 7a), $Re_{2,is} = 1.5 \times 10^5$ (Fig. 7b), and $Re_{2,is} = 3.0 \times 10^5$ (Fig. 7c) respectively. In the entire analyzed Reynolds number range, the misrepresentation of the wake loss profiles shown by the Baseline model results appears to be largely ameliorated when adopting machine-learnt EARSMs. As the difference in the trailing edge momentum thickness values provided by the two RANS computations is small (Fig. 5b), we can conclude that the improvement in wake mixing brought about by the EARSM closures is mostly responsible for such a behaviour. The most striking differences between RANS predictions are recorded at the lowest Reynolds number ($Re_{2,is} = 0.7 \times 10^5$, Fig. 7a). The GEP model already provides a relevant improvement in the reproduction of both the peak loss value and the pitchwise wake width over the Baseline results. However, as observed in previous investigations [18], discrepancies are still visible in the wake periphery region. When the MEMO model is adopted, the representation of wake periphery also improves, especially in the wake half-width coming from the blade suction side. As already observed when discussing the MEMO model training outcomes [23], this is the result of the simultaneous, combined, generation of the transition and EARSM models. As argued in the discussion of the blade surface C_p distributions (Fig. 3), the adoption of the MEMO model improves the base pressure predicted by RANS, as compared with the LES reference data. The feedback between the state of the boundary-layers coming from the blade and wake mixing, that occurs in the combined closure creation process, contributes to enhanced accuracy in the reproduction of the wake loss profile details. Calculations were also carried out by using an ad-hoc wake demarcation strategy based on a threshold on the axial coordinate, so that EARSMs were activated only downstream the trailing edge. It is worthwhile to point out how no difference was observed between wake loss profiles predicted with such a strategy or with the automated one provided by the wake sensing function. As described in [23], the sensing function works in an on/off fashion relative to the application of the EARSMs, and this comparison demonstrates the effectiveness of this approach in completely demarkating the wake affected region. For the $Re_{2,is} = 0.7 \times 10^5$ case, the scaled integrated mixed out C_{pt} values were found to be equal to 1.61, 1.64, and 1.646 for the Baseline, GEP, and MEMO calculations respectively. The scaling term is the experimental (area averaged) C_{pt} at $Re_{2,is} = 1.5 \times 10^5$. The higher mixed-out C_{pt} values suggest a higher level of maturity of the wakes predicted by machine-learnt models relative to the Baseline one. Very similar trends were observed for the other Reynolds numbers.

Unsteady Results

Time-varying inlet boundary conditions for URANS analyses were extracted from LES calculations in an axial section located at $30\%C_x$ upstream the cascade leading edge. Forty instantaneous pitchwise distributions of inlet flow angle, total pressure, and TKE were taken from phase-averaged results and assigned at the inlet boundary of the URANS computational domain. The pitchwise distributions of specific dissipation rate ω was established by using a mixing length formulation: $\omega = \alpha\sqrt{k}/\ell$. In practice, the value of mixing length ℓ was assumed equal to the bars diameter and the constant α was adjusted to ensure the correct TKE decay upstream the blade leading edge. The fulfillment of such a condition was checked, for each considered transition/turbulence model, by comparing instantaneous TKE distributions calculated by RANS at the blade leading edge with ones predicted by LES.

Figure 8 shows instantaneous isolines of TKE superimposed on wake sensing function color contours. It is apparent how the sensing function does a good job in demarcating wake-affected regions in the entire computational domain. Obviously, as can be inferred from Fig. 8, the blade boundary layer is excluded from the application region of machine-learnt EARSMs for two reasons: to avoid turbulent portions of the boundary layer to be affected by anisotropic terms that are not trained for near-wall turbulence, and to preserve laminar flow prior to transition.

Actually, both the GEP and MEMO models have proven to be robust and reliable. The baseline model required 4 wake passing periods to reach a periodic solution, while 6 periods were needed by the machine-learnt transition/turbulence models. So, the computational overhead associated with the use of them is acceptable and compatible with industrial applications. Despite the on/off fashion by which the wake sensing function controls the application of the EARSMs, computational instabilities chargeable to this strategy were actually not observed.

Figure 9 compares the phase-averaged TKE field extracted from the LES solution (Fig. 9a) with instantaneous TKE contours from URANS calculations with the Baseline (Fig. 9b), and MEMO models (Fig. 9c), for a selected phase of the wake passing period. The GEP solution is not reported since, in terms of TKE contours, it is not distinguishable from the MEMO one. The application of the machine-learnt EARSM improves the agreement between URANS and LES both in the chopped wake segments as they migrate through the blade passage (regions indicated with A in Fig. 9) and the transitional/turbulent boundary layer portion on the blade suction side (regions B). Similar results were obtained by looking at other phases different from the one reported in Fig. 9. As discussed by Michelassi and Wissink [11], an amplification of the TKE usually occurs at the bow apex of the wake. Such a feature cannot be captured by turbulence models based on a linear constitutive law that wrongly assumes the strain rate and turbulent stress tensors are aligned. Although the anisotropy introduced by EARSMs models trained for wake mixing hardly matches the one that develops in this region, Fig. 9a and Fig. 9c show such an increase of TKE in region A, while Fig. 9b does not. This is expected to be the result of the non-linear constitutive laws that characterize GEP and MEMO EARSMs.

In order to discuss the unsteady transition pattern as reproduced by URANS, space-time plots of intermittency along the blade suction side, obtained with the Baseline, GEP and MEMO models, are compared in Fig. 10. In the context of laminar kinetic energy based transition models an intermittency factor can be defined as: $\gamma = k/(k_\ell + k)$. In the pretransitional portion of the boundary layer only k_ℓ can be present while k is practically equal to zero, as is for γ. When transition occurs k starts to increase while k_ℓ decreases and γ approaches the unity value as the flow tends to become fully turbulent. This definition has been used in the space-time plots of Fig. 10. The triangular-like region marked with ① represents the wake induced turbulent strip [3], while ② indicates the zone of the space-time diagram located between two subsequent wake related events. The plots of Fig. 10 reveal a neat distinction between the wake induced transitional path and the path between wakes, indicating that all the considered models capture a convincing unsteady transition dynamics. For the Baseline model (Fig. 10a), such a fact was already pointed out by Pacciani et al. [38] through a URANS study on the T106A cascade with incoming bar wakes. The Baseline (Fig. 10a) and GEP (Fig. 10b) models predict similar unsteady transition patterns. The first traces of wake-induced transition appear at $s/s_{tot} \simeq 0.5$, but relevant intermittency values, associated with a boundary layer that becomes turbulent, are encountered only after the 75% of the suction side length. The calmed region [3], namely the region of laminar and attached flow that forms between to subsequent wake passings extends up to the trailing edge. The space-time diagram obtained with the MEMO model (Fig. 10c) shows a particular and fast-pacing transition dynamics. In the MEMO calculation, the suction side boundary layer is exposed to the TKE amplification observed when discussing Fig 9. This, together with an arguably increased sensitivity to incoming wakes turbulence with respect to the Baseline and GEP models, results in a higher level of boundary-layer intermittency prior to wake-induced transition (region 3). This is assumed to be the reason why wake-induced transition appears earlier with respect to the predictions of the other two models. In fact, the wake induced transitional strip originates at approximately 60% of the suction side length, even if with a very gradual evolution towards fully turbulent flow. Also the TKE decrease that occurs, in region 2, as the boundary-layer tends to relax to its pre-transitional state, is seen to be more gradual. Moreover, in contrast again to what can be observed in Figs. 10a and 10b, the intermittency contours in the path between wakes reveal a smooth steady-flow-like transition developing in approximately the last 10% on the blade suction side. Between two subsequent wake passing events, the laminar-boundary layer that exists between the corresponding wake-induced strips undergoes separation. The separation and reattachment lines, deduced from space-time diagrams of wall shear stress, are indicated with S and R in Fig. 10.

In order to gain further insights on the unsteady transition mechanisms reproduced by the different models, a comparison between URANS and LES predictions, in terms of temporal and phase averaged evolutions of the boundary layer shape factor over one wake passing, at $s/s_{tot} = 0.8$, is carried out in Fig. 11. Such a comparison shows how the MEMO model predicts an oscillation amplitude of H_{12} which is lower and more in line with the one predicted by LES with respect to the Baseline and GEP results.

Further information can be deduced from the comparison of time-averaged URANS and LES results in terms of wall-shear stress and boundary layer integral parameters. To this end, Fig. 12 compares distributions of wall shear-stress on the blade suction side. LES predicts a τ_w distribution that remains greater than zero on the whole blade suction side, thus showing no residual separation as a consequence of wake/boundary-layer interaction. Rather, it flattens starting from $s/s_{tot} = 0.7$ up to the blade trailing edge. This is the region where the most striking differences occur in URANS predictions. Here the Baseline model predicts the lowest level of wall shear-stress, with the computed distribution reaching zero at approximately $s/s_{tot} = 0.85$. The MEMO prediction shows the best agreement with LES, while the GEP τ_w distribution lies in between this and the Baseline ones.

Figure 13a compares URANS and LES time-averaged distributions of boundary-layer shape factor on the blade suction side. Differently from the steady case (Fig. 5), where the shape factor remains flat with typical laminar values in the first 60% of the blade suction surface length, the LES time-average distribution shows a monotone decrease of H_{12} from the leading edge up to $s/s_{tot} = 0.5$. Then a peak is found at approximately $s/s_{tot} = 0.7$, which is followed by a drop in H_{12} that tends to reach turbulent values in the last 30%

of the suction side length. The MEMO simulation is the only one among the URANS approaches to resemble such a behaviour in the H_{12} distribution. This is suspected to be related to the more pronounced sensitivity to incoming wake turbulence this model exhibits with respect to the GEP and Baseline models (see the discussion of Fig. 10), a characteristic that probably results in a perturbed laminar boundary state that is similar to the one predicted by LES. Differences arise after the peak, where LES predicts a shape factor that drops with an almost constant slope, while H_{12} calculated with MEMO decreases more slowly up to $s/s_{tot} = 0.9$ and drops rapidly right after. The Baseline and GEP models predict an almost flat H_{12} distribution in the laminar portion of the boundary layer and a too much pronounced peak. These observations, together with the ones reported for the suction surface distributions of wall shear-stress (Fig. 12), reinforce the belief that the MEMO model is the one that reproduces the most realistic unsteady transition dynamics, among the considered transition/turbulence models. Figure 13b shows the comparison between time-averaged boundary layer momentum thickness distributions on the blade suction side. URANS calculations shows very similar trends in the spatial growth rate of the time-averaged momentum thickness. Such trends are different from the one shown by LES in the first 50% of the suction side length, but they become similar to it afterwards. The MEMO model gives the best agreement with the LES distribution, and it yields the maximum momentum thickness at the trailing edge, the Baseline models yields the minimum one, while the GEP model result lies between the other two. In a time-averaged sense, it is then expected that the suction side boundary layer total pressure loss calculated by MEMO and LES are very similar.

There is no significant difference in the predictions by URANS models in terms of time-averaged blade loading, as shown in Fig. 14, where computed blade surface pressure coefficient distributions are compared to the measured one. Consistently with what was observed for the wall shear-stress (Fig. 12), no evidence of a residual separation can be inferred from calculated and experimental C_p distributions that agree fairly well on the entire blade surface.

Computed time-averaged pitchwise distributions of total pressure loss coefficient in the wake $33\%C_x$ downstream of the cascade trailing edge are compared to measurements in Fig. 15. The observations that can be made from this comparison are similar to the ones made for the steady cases (Fig. 7). The Baseline model results look substantially off, with an overestimated loss peak and underestimated wake diffusion. Even freestream losses (i.e. losses outside the wake region) show a different behaviour relative to experiments. The application of machine-learnt models yields a huge difference in the reproduction of the wake structure, with an almost perfect capturing of the loss peak and a much more realistic wake diffusion. The application of the GEP EARSM tends to overdiffuse the wake that appears larger than the experimental one and this is expected to result in an overestimation of mixing losses. It is believed that the application of GEP EARSMs to wake-affected regions of the flowfield, without any modification of the base transition/turbulence closure, results in a modellization that is still too crude for an accurate representation of unsteady wake/blade interaction effects on mixing loss generation. The application of the MEMO model further improves the wake loss profile prediction. There is still evidence of a slight wake overdiffusion, but now both the wake width and freestream losses appear in better agreement with experiments. In terms of mixed-out loss coefficients, the difference between the Baseline and the machine-learnt models predictions is similar to the one detected in the steady case, but now, consistently with its overdiffusing character, the maximum value is obtained from the GEP calculation.

A survey of the loss prediction capabilities of the URANS frameworks is synthesized in Fig. 16, where integrated total pressure loss coefficients are reported as functions of the exit isentropic Reynolds numbers (i.e. the cascade lapse rates). The comparison with experimental data in the steady case shows that the application of machine-learnt models ameliorates loss prediction over the Baseline results at all the considered Reynolds number. However, the most striking improvements are recorded at low Reynolds numbers where the Baseline model tends to underestimate losses due to misrepresentation of wake mixing. When integrated over the cascade pitch, wake loss profiles obtained with GEP and MEMO models yields extremely similar values of total pressure loss coefficients, with MEMO results slightly closer to measured data. Experiments show how the presence of the incoming wakes, with the tested reduced frequency value, results in a relevant increase in losses. Such a behaviour of the integrated loss is reproduced by all the URANS frameworks, but with different magnitudes. The Baseline model yields the smallest increase in total pressure loss coefficient in unsteady inlet flow conditions, probably due to the combined effect of underestimated trailing edge momentum thickness (see Fig. 13b) and wake mixing (Fig. 15). The GEP and MEMO predictions are consistent with the results of Fig. 15 with a loss level closer to the experimental one. Although the assessment of unsteady results is carried out only at $Re_{2,is} = 0.7 \times 10^5$, it can be argued that the zonal application of combined transition/turbulence machine-learnt closures is a promising way to improve the predictive capabilities of URANS approaches for unsteady interaction effects in LPTs.

CONCLUSIONS

Two different transition/turbulence models, developed by a data-driven machine-learning techniques based on the GEP algorithm, have been validated through the study of a LPT cascade, representative of state-of-the-art design, under steady and unsteady inflow conditions. The first one (GEP) consists in the application of a machine-learnt EARSM closure created for improved wake mixing predictions in LPTs on top of the baseline $k_\ell - k - \omega$ model by Pacciani et al. [9, 24, 25]. The second one (MEMO) is based on a fully coupled transition and EARSM closure, with the transition and turbulence model components simultaneously trained via a multi-expression, multi-objective GEP-based technique. The considered models are applied, in both steady and unsteady inflow conditions, in a fully automated fashion via the use of a wake/boundary-layer sensing function. Precursor LES calculations were carried out, by means of the STAR-CCM+ code, in both steady and unsteady inflow conditions, at ($Re_{2,is} = 07 \times 10^5$).

The computational framework comprising GEP and MEMO models has proven to be robust and reliable. Steady and unsteady calculations were carried out without any relevant user adjustment in model or sensing function parameters. The computational overhead associated with the use of the machine learnt models is almost negligible and in line with an industrial use of the numerical framework.

Striking improvements resulted from the application of machine-learnt closures in the prediction of blade surface distribution of loading, wall-shear stress, boundary-layer integral parameters and, mostly, in the wake structure reproduction. This is true in both steady and unsteady inflow cases. The best agreement with experiments and LES results is shown by the MEMO closure that improves not only the centerline prediction, but also the reproduction of the wake peripheral region, where the GEP closure still lacks accuracy. In the wake, the level of agreement with measurements is non uniform through the analyzed Reynolds number range indicating that there is still scope for improvement in the closures. This can probably be achieved by extending the multi-expression, multi-objective GEP technique towards a multi-case training capability.

In the unsteady inflow case, the application of the EARSMs in wake-affected regions upstream, inside the blade passage, and downstream of the cascade trailing edge has proven to improve URANS predictions of the instantaneous TKE flowfield, as compared with LES results.

A close agreement with measurements was recorded in terms of wake total pressure coefficient profiles for the MEMO model. In contrast, the GEP model, resulted in an overdiffusion of the wake. It is concluded that, even in unsteady wake/blade interaction cases, if the state of the boundary-layers coming off the blade is more accurately represented, the wake mixing prediction also improves.

In terms of steady cascade lapse rates, the application of machine-learnt models is seen to ameliorate the loss prediction, over the Baseline results, at all the considered Reynolds numbers. The most striking improvements are recorded at low Reynolds numbers where the Baseline model tends to underestimate losses due to misrepresentation of wake mixing. Although the correct trend in loss changes, when unsteady inflow is considered, is captured by all the URANS frameworks, machine-learnt closures tend to give better agreement with measurements with respect to the Baseline one. Comparisons between calculated and measured data show that there is still scope for improvement in machine-learnt transition/turbulence closures. However, this study demonstrates how GEP-based machine-learning techniques for the combined development of transition and turbulence models represent a very promising strategy for further improve RANS/URANS flow calculations in LPTs. The discussed results show how closures generated with the multi-expression, multi-objective approach are already quite close to challenging LES analyses in terms of boundary layer and wake reproduction. The extension of the multi-expression, multi-objective GEP technique towards a multi-case capability, possibly including unsteady analyses in the training process, is expected to further narrow the gap that still exists between URANS and High-Fidelity predictive capabilities. This open also the possibility of further generalize the model by extending the training to different geometries and flow conditions like, for example, the ones that characterize High Pressure turbines.

ACKNOWLEDGMENT

The authors would like to thank GE Avio for the permission of publishing this paper. The University of Florence acknowledges the contribution of the National Recovery and Resilience Plan, Mission 4 Component 2 - Investment 1.4 - Italian Research Center on High Performance Computing, Big Data and Quantum Computing - funded by the European Union - NextGenerationEU - (CUP B83C22002830001). R. D. Sandberg acknowledges funding from the Australian Research Council Future Fellowship (Grant FT190100072). The authors would also like to thank Ms. Federica Mugnaioni for her precious help in carrying out calculations.

NOMENCLATURE

C	Blade chord length
$C_p = \frac{p_{01}-p}{p_{01}-p_2}$	Pressure coefficient
$C_{pt} = \frac{p_{01}-p_0}{p_{01}-p_2}$	Total pressure loss coefficient
H_{12}	Boundary-layer shape factor
k	Turbulent kinetic energy
k_ℓ	Laminar kinetic energy
ℓ_T	Inlet turbulence length scale
p	Fluid pressure
Re	Reynolds number
s	Curvilinear abscissa along blade surface
U	Peripheral velocity
V	Velocity magnitude
x, y	Cartesian coordinates
y	Wall distance
γ	Intermittency
τ_w	wall-shear stress
ω	specific turbulence dissipation rate

Ω	Vorticity magnitude
θ	Boundary-layer momentum thickness

SUBSCRIPTS / SUPERSCRIPTS

0	Total quantity
1	Inlet
2	Outlet
ref	Reference
x	Axial
tot	Total
T	Turbulent
ℓ	Laminar

ACRONYMS

CFD	Computational fluid dynamics
DNS	Direct numerical simulation
EARSM	Explicit algebraic Reynolds stress model
FSTI	Free-stream turbulence intensity
GEP	Gene expression programming
LKE	Laminar kinetic energy
LES	Large eddy simulation
LPT	Low pressure turbine
MEMO	Multi-expression and multi-objective
NDA	Non disclosure agreement
RANS	Reynolds averaged Navier-Stokes
TKE	Turbulent kinetic energy
TVD	Total variation diminishing
URANS	Unsteady RANS

REFERENCES

[1] Michelassi, V., Chen, L. W., Pichler, R., and Sandberg, R. D., 2015. "Compressible Direct Numerical Simulation of Low Pressure Turbine - Part II: Effect of Inflow Disturbances". *J. Turbomach.,* ***137***(7), p. 71005.

[2] Stieger, R. D., and Hodson, H. P., 2005. "The Unsteady Development of a Turbulent Wake Through a Downstream Low-Pressure Turbine Blade Passage". *J. Turbomach.,* ***127***(2), p. 388.

[3] Hodson, H. P., and Howell, R. J., 2005. "Bladerow Interactions, Transition, and High-Lift Aerofoils in Low-Pressure Turbines". *Annu. Rev. Fluid Mech.,* ***37***, pp. 71–98.

[4] Praisner, T. J., Clark, J. P., Nash, T. C., Rice, M. J., and Grover, E. A., 2006. "Performance Impacts Due to Wake Mixing in Axial Flow Turbomachinery". In Proc. of the ASME Turbo Expo, Vol. 6: Turbomachinery, Parts A and B, pp. 1821–1830.

[5] Sandberg, R. D., and Michelassi, V., 2021. "Fluid dynamics of axial turbomachinery: Blade-and stage-level simulations and models". *Annual Review of Fluid Mechanics,* ***54***.

[6] Sandberg, R. D., and Michelassi, V., 2019. "The current state of high-fidelity simulations for main gas path turbomachinery components and their industrial impact". *Flow Turbul. Combust.,* ***102***, pp. 797–848.

[7] Dick, E., and Kubacki, S., 2017. "Transition Models for Turbomachinery Boundary Layer Flows: A Review". *Int. J. Turbomach. Propuls.,* ***2***(2), p. 4.

[8] Walters, D. K., and Cokljat, D., 2008. "A Three-Equation Eddy-Viscosity Model for Reynolds-Averaged Navier-Stokes Simulations of Transitional Flow". *J. Fluids Eng.,* ***130***(12), p. 121401.

[9] Pacciani, R., Marconcini, M., Fadai-Ghotbi, A., Lardeau, S., and Leschziner, M. A., 2011. "Calculation of High-Lift Cascades in Low Pressure Turbine Conditions Using a Three-Equation Model". *J. Turbomach.,* ***133***(3), p. 031016.

[10] Marconcini, M., Pacciani, R., Arnone, A., Michelassi, V., Pichler, R., Zhao, Y., and Sandberg, R., 2019. "Large Eddy Simulation and RANS Analysis of the End-Wall Flow in a Linear LPT Cascade with Variable Inlet Conditions, Part II: Loss Generation". *J. Turbomach.,* ***141***(5), p. 051004.

[11] Michelassi, V., and Wissink, J. G., 2015. "Turbulent Kinetic Energy Production in the Vane of a Low-Pressure Linear Turbine Cascade with Incoming Wakes". *International Journal of Rotating Machinery,* ***2015***(650783), pp. 1–15.

[12] Duraisamy, K., 2021. "Machine Learning Augmented Reynolds-Averaged & Large Eddy Simulation Models of Turbulence". *arXiv*. 2009.10675v3.

[13] Weatheritt, J., and Sandberg, R. D., 2016. "A Novel Evolutionary Algorithm Applied to Algebraic Modifications of the RANS

Stress-Strain Relationship". *J. Comput. Phys.,* ***325***, pp. 22–37.

[14] Ferreira, C., 2001. "Gene Expression Programming: a New Adaptive Algorithm for Solving Problems". *Complex Systems,* ***13***(2), pp. 87–129.

[15] Akolekar, H. D., Sandberg, R. D., Hutchins, N., Michelassi, V., and Laskowski, G., 2019. "Machine-Learnt Turbulence Closures for Low Pressure Turbines with Unsteady Inflow Conditions". *J. Turbomach.,* ***141***(10), p. 101009.

[16] Akolekar, H. D., Weatheritt, J., Hutchins, N., Sandberg, R. D., Laskowski, G., and Michelassi, V., 2019. "Development and Use of Machine-Learnt Algebraic Reynolds Stress Models for Enhanced Prediction of Wake Mixing in Low-Pressure Turbines". *J. Turbomach.,* ***141***(4).

[17] Akolekar, H. D., Zhao, Y., Sandberg, R. D., Hutchins, N., and Michelassi, V., 2019. "Turbulence Model Development for Low & High Pressure Turbines Using a Machine Learning Approach". In ISABE Conf. Proc. paper 2019-24010.

[18] Pacciani, R., Marconcini, M., Bertini, F., Taddei, S. R., Spano, E., Akolekar, H. D., Sandberg, R. D., and Arnone, A., 2021. "Assessment of machine-learnt turbulence models trained for improved wake-mixing in low pressure turbine flows". *Energies,* ***14***(24), p. 8327.

[19] Zafar, M. I., Xiao, H., Choudhari, M. M., Li, F., Chang, C. L., Paredes, P., and Venkatachari, B., 2020. "Convolutional Neural Network for Transition Modeling Based on Linear Stability Theory". *Phys. Rev. Fluids,* ***5***(11), pp. 1–15.

[20] Yang, M., and Xiao, Z., 2020. "Improving the k- ω - γ -Ar Transition Model by the Field Inversion and Machine Learning Framework". *Phys. Rev. Fluids,* ***32***(6).

[21] Akolekar, H. D., Waschkowski, F., Zhao, Y., Pacciani, R., and Sandberg, R. D., 2021. "Transition Modeling for Low Pressure Turbines Using CFD-Driven Machine Learning". *Energies,* ***14***(15), p. 4680.

[22] Zhao, Y., Akolekar, H. D., Weatheritt, J., Michelassi, V., and Sandberg, R. D., 2020. "RANS Turbulence Model Development Using CFD-Driven Machine Learning". *J. Computat. Phys.,* ***411***, p. 109413.

[23] Akolekar, H. D., Pacciani, R., Waschkowsky, F., Zhao, Y., and Sandberg, R. D., 2022. "Multi-objective development of machine-learnt closures for fully integrated transition and wake mixing predictions in low pressure turbines". *ASME Paper GT2022-81091*.

[24] Pacciani, R., Rubechini, F., Arnone, A., and Lutum, E., 2012. "Calculation of Steady and Periodic Unsteady Blade Surface Heat Transfer in Separated Transitional Flow". *J. Turbomach.,* ***134***(6), p. 061037.

[25] Pacciani, R., Marconcini, M., Arnone, A., and Bertini, F., 2014. "Predicting High-Lift Low-Pressure Turbine Cascades Flow Using Transition-Sensitive Turbulence Closures". *J. Turbomach.,* ***136***(5), p. 051007.

[26] Simoni, D., Berrino, M., Ubaldi, M., Zunino, P., and Bertini, F., 2015. "Off-Design Performance of a Highly Loaded LP Turbine

Cascade Under Steady and Unsteady Incoming Flow Conditions". *J. Turbomach.,* ***137***(7), p. 071009.

[27] Marconcini, M., Pacciani, R., Arnone, A., and Bertini, F., 2015. "Low-Pressure Turbine Cascade Performance Calculations With Incidence Variation and Periodic Unsteady Inflow Conditions". *ASME paper GT2015-42276*.

[28] Arnone, A., 1994. "Viscous analysis of three-dimensional rotor flow using a multigrid method". *J. Turbomach.,* ***116***(3), pp. 435–445.

[29] Chorin, A. J., 1967. "A Numerical Method for Solving Incompressible Viscous Flow Problems". *J. Comput. Phys.,* ***2***, pp. 12–26.

[30] Pacciani, R., Marconcini, M., and Arnone, A., 2019. "Comparison of the AUSM$^+$-up and Other Advection Schemes for Turbomachinery Applications". *Shock Waves,* ***29***(5), pp. 705–716.

[31] Arnone, A., Pacciani, R., and Sestini, A., 1995. "Multigrid Computations of Unsteady Rotor–Stator Interaction Using the Navier–Stokes Equations". *Journal of Fluids Engineering,* ***117***, December, pp. 647–652.

[32] Arnone, A., and Pacciani, R., 1997. "Numerical Prediction of Trailing Edge Wake Shedding". *ASME paper 97-GT-89*. ASME Turbo Expo, June 2–5, Orlando, FL, USA.

[33] Burberi, C., Michelassi, V., Scotti Del Greco, A., Lorusso, S., Tapinassi, L., Marconcini, M., and Pacciani, R., 2020. "Validation of Steady and Unsteady CFD Strategies in the Design of Axial Compressors for Gas Turbine Engines". *Aerosp. Sci. and Technol.,* ***107***(106307).

[34] Wilcox, D. C., 2006. *Turbulence Modeling for CFD*, 3rd ed. DCW Industries Inc., La Canada, USA.

[35] Pope, S. B., 1975. "A More General Effective-Viscosity Hypothesis". *Journal of Fluid Mechanics,* ***72***(2), pp. 331–340.

[36] Nicoud, F., and Ducros, F., 1999. "Subgrid-scale stress modelling based on the square of the velocity gradient tensor". *Flow, Turbulence and Combustion,* ***62***, pp. 183–200.

[37] Benamadouche, S., Jarrin, N., Addad, Y., , and Laurence, D., 2006. "Synthetic turbulent inflow conditions based on a vortex-method for large eddy simulation". *Progress in Computational Fluid Dynamics,* ***6***, pp. 50–57.

[38] Pacciani, R., Marconcini, M., Arnone, A., and Bertini, F., 2014. "Predicting High-Lift LP Turbine Cascades Flows Using Transition-Sensitive Turbulence Closures". *J. Turbomach.,* ***136***(5), p. 051007.

LIST OF TABLES

TABLE 1: Mesh sizes for the grid dependency analysis.

G1	G2	G3
321×65	621×101	1201×201

LIST OF FIGURES

(b) (turbo-23-1186-fig13b)

Figure 14: Measured and computed time-averaged C_p distributions ($Re_{2,is} = 0.7 \times 10^5$). (turbo-23-1186-fig14)

Figure 15: Measured and computed time-averaged wake total pressure loss profile ($x/C_x = 1.33$, $Re_{2,is} = 0.7 \times 10^5$). (turbo-23-1186-fig15)

Figure 16: Steady and unsteady cascade lapse rates ($x/C_x = 1.33$). (turbo-23-1186-fig16)

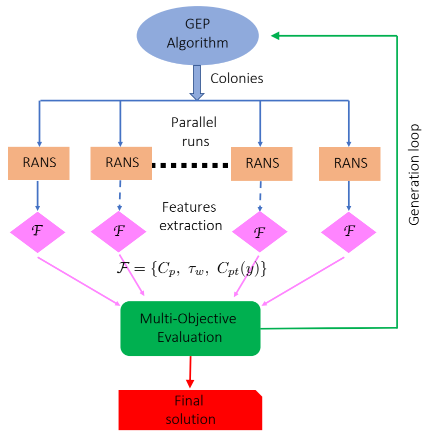

FIGURE 1: Sketch of the CFD-driven GEP algorithm.

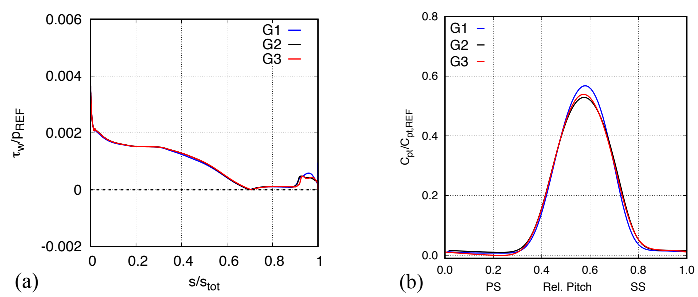

FIGURE 2: Computed wall shear-stress distributions (a), and wake loss profiles (b), at $Re_{2,is} = 0.7 \times 10^5$ for G1, G2, and G3 grids.

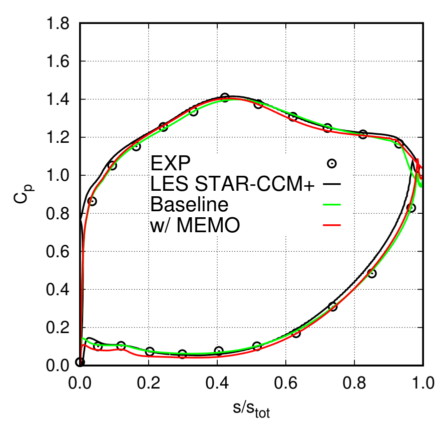

FIGURE 3: Computed and experimental C_p distributions at $Re_{2,is} = 0.7 \times 10^5$.

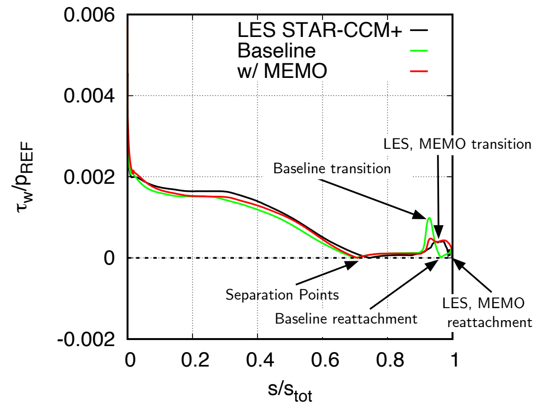

FIGURE 4: RANS and LES τ_w distributions at $Re_{2,is} = 0.7 \times 10^5$.

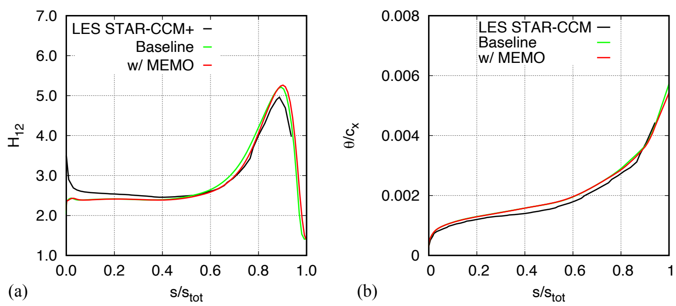

FIGURE 5: RANS and LES H_{12} (a), and θ (b) distributions at $Re_{2,is} = 0.7 \times 10^5$.

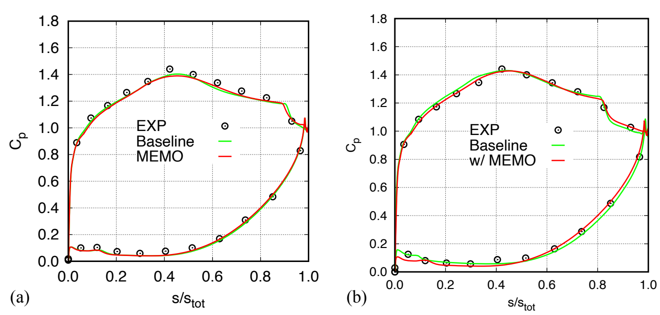

FIGURE 6: Computed and experimental C_p distributions at $Re_{2,is} = 1.5 \times 10^5$ (a), and $Re_{2,is} = 3.0 \times 10^5$ (b).

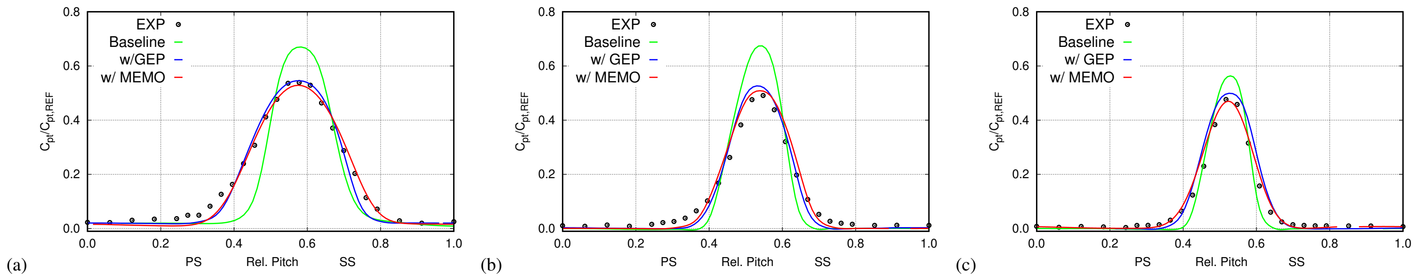

FIGURE 7: Computed and experimental wake total pressure loss profiles at $Re_{2,is} = 1.5 \times 10^5$ (a), and $Re_{2,is} = 3.0 \times 10^5$ (b) $(x/C_x = 1.33)$.

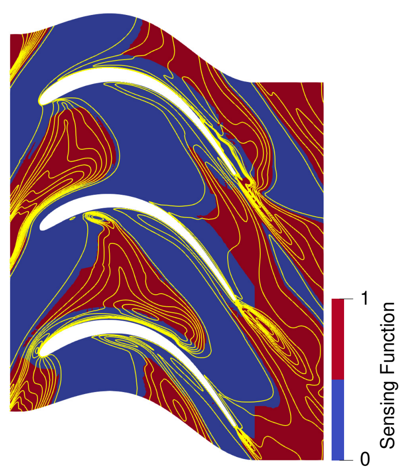

FIGURE 8: Non-dimensional TKE isolines overimposed on color contours of wake sensing function ($Re_{2,is} = 0.7 \times 10^5$).

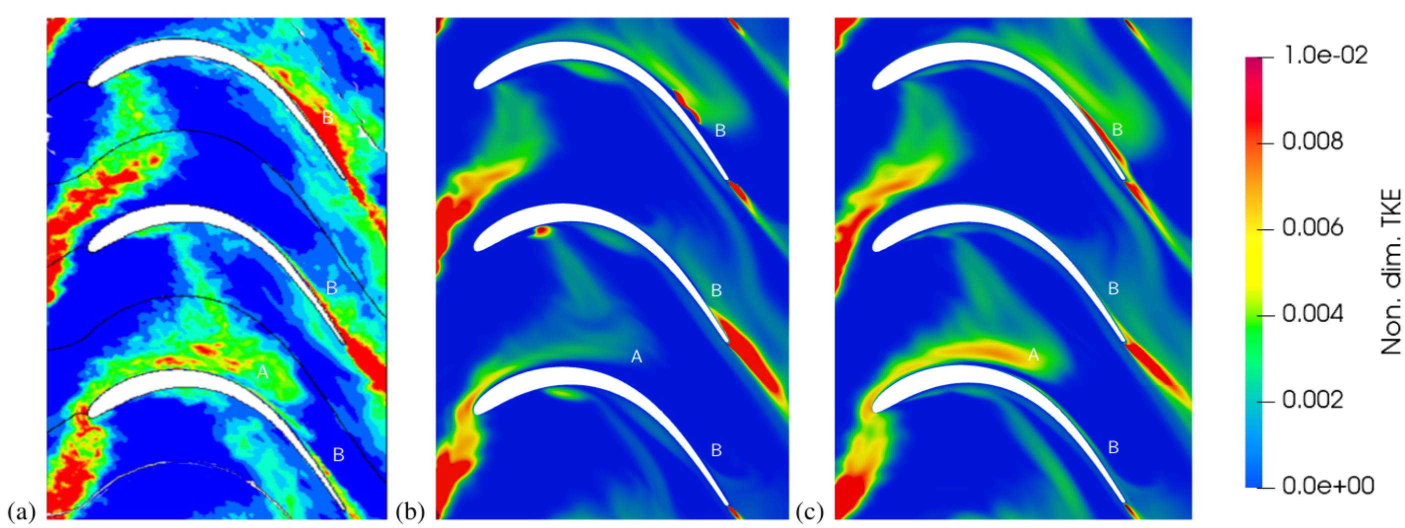

FIGURE 9: Instantaneous TKE fields: LES (a), BSL (b), MEMO (c) ($Re_{2,is} = 0.7 \times 10^5$).

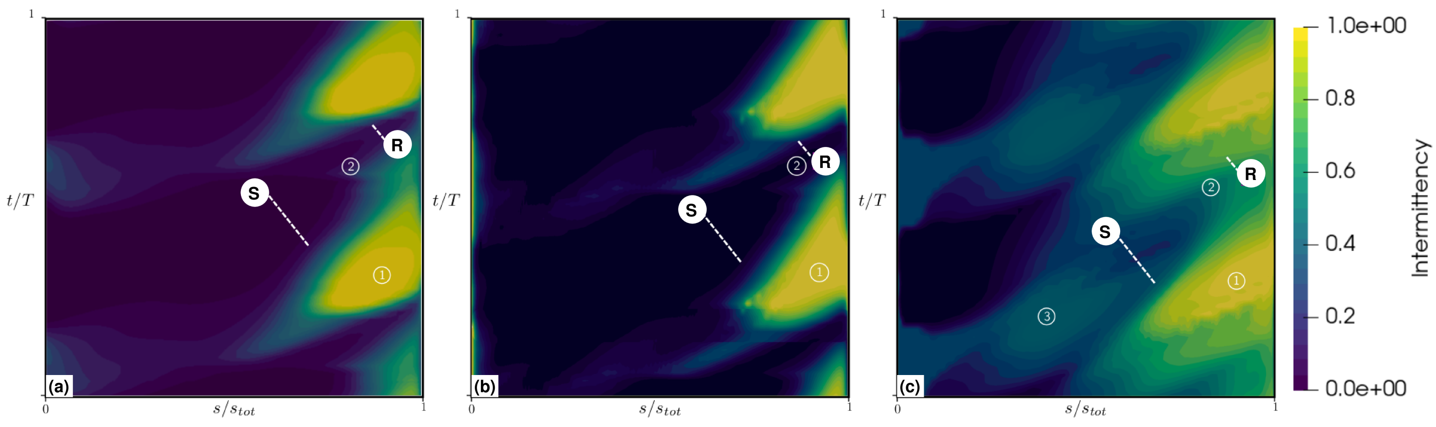

FIGURE 10: Space-time contours of intermittency on the blade suction side: BSL (a), GEP (b), MEMO (c) ($Re_{2,is} = 0.7 \times 10^5$).

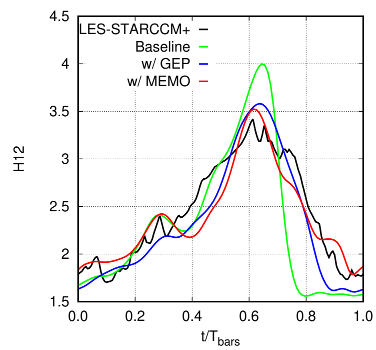

FIGURE 11: Time evolutions of H_{12} at $s/s_{tot} = 0.8$ ($Re_{2,is} = 0.7 \times 10^5$).

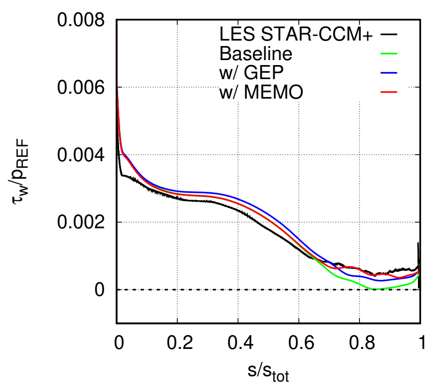

FIGURE 12: Time-averaged suction surface distributions of τ_w ($Re_{2,is} = 0.7 \times 10^5$).

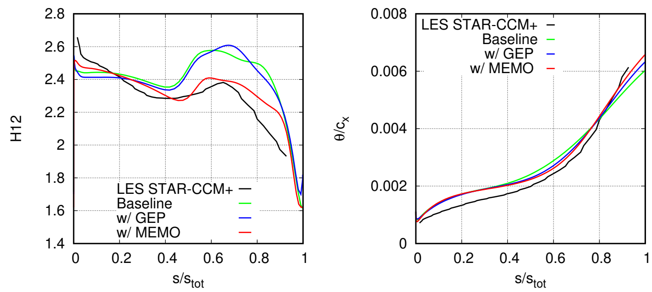

(a) (b)

FIGURE 13: Time-averaged suction surface H_{12} (a) and θ (b) distributions ($Re_{2,is} = 0.7 \times 10^5$).

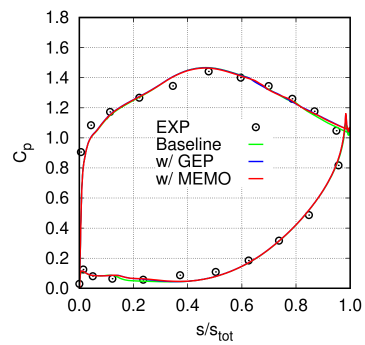

FIGURE 14: Measured and computed time-averaged C_p distributions ($Re_{2,is} = 0.7 \times 10^5$).

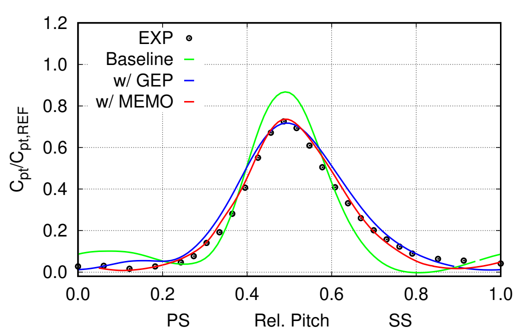

FIGURE 15: Measured and computed time-averaged wake total pressure loss profile ($x/C_x = 1.33$, $Re_{2,is} = 0.7 \times 10^5$).

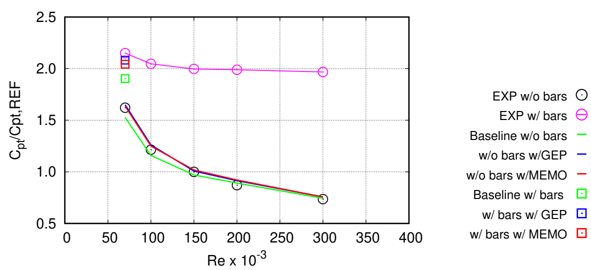

FIGURE 16: Steady and unsteady cascade lapse rates ($x/C_x = 1.33$).